Crescent singularities and stress focusing in a buckled thin sheet: Mechanics of developable cones

Sahraoui Chaïeb* and Francisco Melo
Departamento de Física de la Universidad de Santiago, Avenida Ecuador 3493, Casilla 307, Correo 2, Santiago, Chile
(Received 27 April 1998; revised manuscript received 18 May 1999)

The localization of deformation is a simple consequence of the fact that bending a thin sheet is energetically cheaper than stretching it. In this paper we investigate conical singularities that appear on a crumpled sheet and called developable cones (*d* cones). We found that for a sample of a finite thickness the singularity is never pointlike but has a spatial extension in the form of a crescent. A further deformation of the *d* cone leads to a transition to a plastic deformation equivalent to a decrease in the singularity size characterized from curvature and profile analysis. The crescent radius of curvature is measured both at small deformations and at large deformations. It is found that, during the buckling process, the curvature of the crescent exhibits two different scalings versus the deformation. From the cone profile, we measured the reaction force of the plate to deformation; and from force measurements, the energy that is necessary to create the singularity is characterized. [S1063-651X(99)09310-1]

PACS number(s): 46.25.Cc, 46.70.−p, 62.20.Fe, 68.55.Jk

I. INTRODUCTION

Strong deformations of membranes and thin shells span a wide range of length scales. On the microscopic scale, quenched disorder in partially polymerized membranes and thermal fluctuations induce, without strain, a crumpling transition at the melting point, below which the membrane behaves like a two-dimensional (2D) solid. At the crumpling transition, partially polymerized vesicles look like dried prunes [1–3]. Some inorganic compounds such as nanotubes were observed in a phase that is similar to a crumpled sheet [4] and could be buckled like macroscopic sheets [5]. At large scale, and in the $(2+1)$ dimensional general relativity, defect-induced deformations of a 2D space-time sheet are characterized by the presence of a conical singularity [6]. In intermediate scales, the stability of shells and thin elastic plates is of great importance in structure engineering and packaging material development [7]. When a thin elastic sheet is confined to a region much smaller than its size, the morphology of the resulting crumpled membrane is a network of straight ridges or folds that meet at sharp points or vertices. Singularities that appear on such a crumpled sheet, as a result of the stress focusing, have recently been the subject of several investigations [8–16]. For instance, in the case of a crumpled sheet, developable cones were found to be the solution to Fopple–von Kármán (FvK) equations for large deflections [9]. In the following we will refer to these singularities as *d* cones. Developable cones are a special class of developable surfaces. Developable surfaces are obtained from, or applied to, a plane, without changing distances. Unlike developable surfaces, a developable cone has a zero Gaussian curvature everywhere except at the tip, called the *singularity*, where the curvature diverges. A scaling analysis of the FvK equations has shown that strain and deformation energy are located within the ridge region that separates two singularities [12]. In practice, it has been shown that singularity energy plays an important role in selecting characteristic lengths in an axially buckled cylindrical sheet. These lengths were shown to be the distance separating two *d* cones [14], whose selection was due to a competition between bending energy, which favors large creases by flattening the surface, and the singularity energy, which favors smaller creases by respecting geometrical constraints like the natural curvature of the cylindrical shell. This linear relation between the crease length and the panel radius found experimentally in [14] was imposed, between the crease length and the radius of a ball made by crumpling an elastic sheet, as a condition to fulfilling the scaling of the deformation energy versus the crease length [11]. In a study of a conical singularity, the shape of a developable cone was calculated from the condition of zero in-plane stress and developability [16]. However, a study of the postbuckling state is still lacking, which could explain the appearance of the irreversible crescent shape of conical singularities in a crumpled sheet [17].

In this paper we study mechanical and topological properties of the crescent singularity left after postbuckling a circular sheet of thickness *h*. Unlike zero thickness sheets studied theoretically, the singularity in a real sheet is not a pointlike vertex, but has a spatial extension over a radius R_c. This crescent appears as a strain-localization-induced curvature focusing at the ridge separating the convex region and the concave region of the *d* cone. This focusing is tested by measuring the growth of the curvature on the ridge and on the concave part. It is also revealed by measuring the reaction force of the plate at the ridge and at the concave part. The *singularity energy* is measured as the energy dissipated when the crescent appears.

This paper begins with a description of the setup. In Sec. III we present the profiles of the *d* cone, from which we retrieve the opening and the aperture angles. In Sec. IV we discuss in more detail a simple model [15] that describes the

*Present address: Room 3-253, Department of Mechanical Engineering, Massachusetts Institute of Technology, 77 Mass. Ave. Cambridge, MA, 02139.

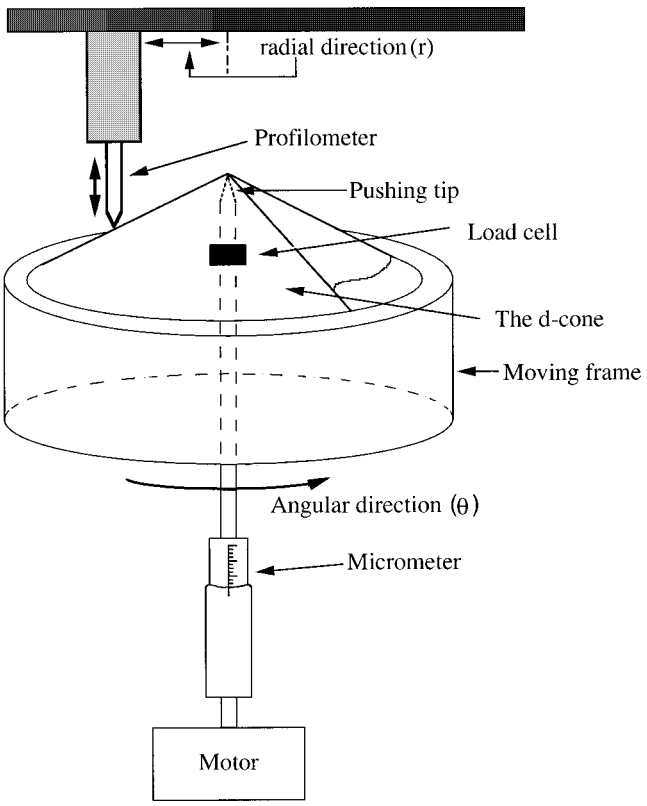

FIG. 1. Setup where the *d* cone is performed and where the profilometric measurements are achieved.

properties of the *d* cone as an isometric deformation obtained by pure bending. In Sec. V, we present and discuss the local properties, topological and mechanical, of the *d* cone. Sections V A, V B and V C are a detailed description of the geometrical model already presented in [15]. In Sec. VI we present force measurements from profiles and from direct load measurements, the latter allowing us to measure the singularity energy. Finally, an eventual analogy between the *d* cone and the dislocation problem is discussed, and future implications are presented in Sec. VII.

II. EXPERIMENTAL SETUP

The *d* cone is obtained on a thin circular plate by pushing a round tip (0.5 mm diameter) into the center of the principal axis of the plate. In this study we used circular plates made from both 0.05- and 0.1-mm-thick sheets (copper, brass, steel, and transparencies or acrylic); the results discussed are mainly from the 0.1-mm-thick sheets. In order for the developable cone to to form, we allow the border of the sheet to move freely in a circular rigid frame while the tip is pushed in. The radius of the frame is 5% smaller than the sample radius R_f (Fig. 1), whose radius ranges from 15 to 90 mm. The opening angle ϕ of the *d* cone (defined as the angle between the horizontal plane and the cone convex part generatrix) is varied by pushing the tip perpendicularly to the circular plate and measuring the displacement *d* using a precision micrometer with a resolution of 10^{-2} mm. A miniature load cell is mounted under the pushing tip so that the force exerted by the plate can be measured. The pushing tip is mounted on a rigid 20-cm-long and 1-cm-thick steel pen-

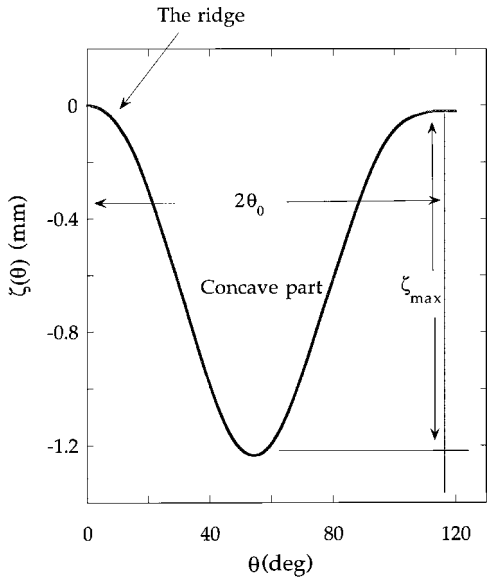

FIG. 2. Profile of the *d* cone in Cartesian coordinates. Notice the angle $2\theta_0$ that measures the aperture angle between the points where the plate loses contact with the frame.

shaped cylinder. This bar is rigid enough to be inflexible when pushing the plate. A profilometric tip, mounted on the active part of a position sensor transducer, enables us to probe the surface of the sheet. Two motors allow the tip to scan the whole plate surface. The first motor moves the tip on a miniature automatic displacement guide mounted along the radial direction and the second motor rotates the frame around its axis. The radial and angular directions are marked in Fig. 1 as (r) and (θ), respectively. The measurement precision of the developable-cone opening angle is approximately 7×10^{-4} rad. The experiment is controlled and data are acquired by a personal computer (PC) equipped with analog-to-digital converter and GPIB boards. In order to avoid stretching the plate when a deformation *d* is imposed, a part of the plate must lose contact with the frame, leading to a concave region whose amplitude increases as *d* increases and whose location is randomly distributed on the plate. If the pushing tip deviates from the center by a distance on the order of a few millimeters, the characteristics of the sheet deflection will not change significantly, but the nucleation of the cone will occur in the region where the pushing tip is closest to the frame border. In some cases, two or four *d* cones appear. Pushing the plate further, only one of the cones remains and its amplitude increases. In the following we present local features of the buckled plate obtained by probing the surface with a profilometer.

III. PROFILES

In order to characterize the local geometry of the *d* cone fully, we built a profilometer (shown in Fig. 1) that consists of a tip connected to a transducer controlling the displacement of the tip. The moving frame that supports the sample can have a very low angular velocity. The profilometer is able to resolve less than 0.01 mm in the vertical (z) and horizontal directions (r,θ). Figure 2 displays the profile obtained at a given distance r from the singularity, and for a given deformation *d*. From this profile, it is possible to mea-

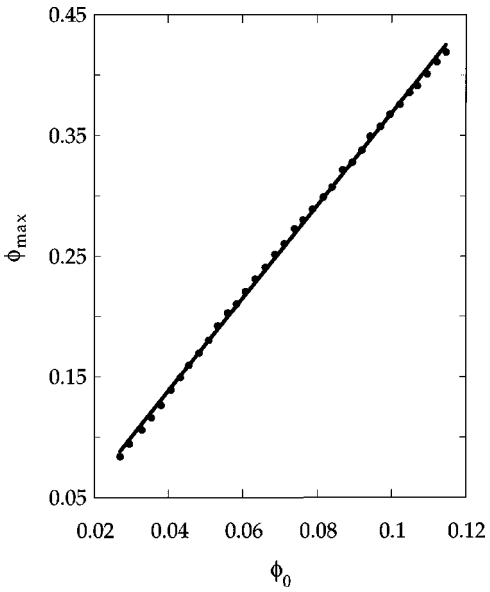

FIG. 3. Plate maximum deflection as a function of the angle between the convex part and the horizontal plane. The distance to the pushing tip is 3 mm.

sure the maximum deflection $\phi_{\max}$ made by the concave region with the horizontal direction as a function of the angle ϕ_0 made by the convex region and the horizontal direction. From Fig. 2 we measured the aperture angle of the deflection in the θ direction. This angle was found to be independent of the plate size and the deformation for a given geometry. Figure 2 displays the maximum deflection and how the angle $2\theta_0$ is measured. The horizontal line corresponds to the convex part of the cone. At high deformations, the two procedures give two different angles. From this figure we measure the maximum deflection $\phi_{\max}$, which is the lowest point in the Fig. 2, with $z_{\max}(\theta)=r\phi_{\max}(\theta)$, where r is the distance measured from the pushing tip. In Fig. 3 we display the dependence of $\phi_{\max}$ versus the deformation expressed by the angle $\phi_0=d/R_f$. The best linear fit to the data in the figure above gives $\phi_{\max}\sim 3.73\phi_0$. We will show in the following section that this selection of aperture angle $2\theta_0$ and maximum deflection as a function of the deformation can be explained by a minimization of the bending energy, taking into account the fact that the deformation is isometric. In polar coordinates, the plate profile looks like the ones displayed in Fig. 4. The $(+)$ sign refers to positive curvature in the convex part and the $(-)$ sign refers to negative curvature in the concave region. Each profile was obtained for a fixed distance from the pushing tip. Figure 4(a), corresponds to profiles of the d cone for small d and for different distances r from the pushing tip, and the profiles for large deformations are shown in Fig. 4(b). It is clear from this figure that the convex part (circular curve in the figure) is off-center. This shift of the d-cone tip will be explained as particular to d cones made from a nonzero thickness sheet.

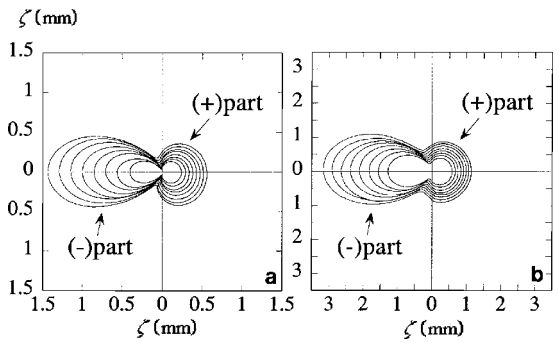

FIG. 4. Contour plot of the sheet profile in polar coordinates vs the angle θ. (a) $d=1.41$ mm; (b) $d=5.48$ mm. The axes are in millimeters. The different curves correspond to different distances from the pushing tip.

IV. ENERGY MINIMIZATION OF AN ISOMETRIC DEFORMATION

In the following we show that a simple model consisting of a minimization of the curvature energy, taking into account the fact that the deformation is isometric, can explain the above results and can describe the d cone far from the singularity. The general equation of a cone centered in O, in cylindrical coordinates, is written as $z=rf(\theta)$. For convenience, we rewrite the parametric equation, $z=r\tan\phi(\theta)$ and $r=R\cos\phi(\theta)$, where R is the distance to the tip and θ is the polar angle. A cone corresponds to a given function $\phi(\theta)$, where ϕ is defined as above. For a given deformation, $\epsilon=d/R_f=\tan\phi_0$, where d is the amount of the micrometer vertical displacement. If we write $\phi(\theta)=\phi_0$, for $|\theta|>\theta_0$,

$$\phi(\theta)=\phi_0+\gamma\left(1+\cos\pi\frac{\theta}{\theta_0}\right) \quad \text{for} \quad |\theta|<\theta_0. \tag{4.1}$$

The function $\phi(\theta)$ defines then a cone that remains in contact with the circular frame for $|\theta|>\theta_0$. The d cone is detached from the plate over an angle equal to $2\theta_0$ that corresponds to the deflection. We assume that d is small and that γ and ϕ_0 are of the same order of magnitude. To first order, the total curvature of the surface then reduces to $\kappa=(\phi+\phi'')/R$. The corresponding energy E_κ (per unit of R) is

$$E_\kappa=\frac{K}{2}\int_{-\pi}^{\pi}\frac{(\phi+\phi'')^2}{R^2}R\sqrt{\cos^2\phi+\phi'^2}\,d\theta$$

$$\sim\frac{K}{2R}\left[2\pi\phi_0^2+4\theta_0\phi_0\gamma+\left(3\theta_0-\frac{2\pi^2}{\theta_0}+\frac{\pi^4}{\theta_0^3}\right)\gamma^2\right]. \tag{4.2}$$

For an unstretchable plate, the length L of the corresponding line at $R=\text{const}$ must be equal to $2\pi R$, so that

$$2\pi R=L=\int_{-\pi}^{\pi}R\sqrt{\cos^2\phi+\phi'^2}\,d\theta$$

$$\sim\left[2\pi-\pi\phi_0^2-2\theta_0\phi_0\gamma-\left(\frac{3\theta_0}{2}-\frac{\pi^2}{2\theta_0}\right)\gamma^2\right]R. \tag{4.3}$$

Equation (4.3) gives γ as a function of ϕ_0 and θ_0. Replacing γ by its value in Eq. (4.2) and minimizing E_κ with respect to θ_0, one finds $2\theta_0\sim 2.09$ rad$\sim 120°$ and $\gamma\sim 1.38\phi_0$. This last relation confirms our assumption that γ

and ϕ_0 are of the same order of magnitude. An exact solution of a similar problem gives $2\theta_0 \sim 140°$ [16]. As pointed out above, our result is valid for low deformations. The theoretical value of the aperture angle $2\theta_0$ is in good agreement with the experiment (Fig. 2). The aperture angle between the points where the plate loses contact with the frame is about $(110 \pm 5)°$. Experimentally, and even for large d, the aperture angle depends very little on d when measured in the plate coordinates. The theoretical maximal deflection angle $\phi_{\max} = \phi(0)$ is proportional to ϕ_0 and equals $\phi(0) = (\phi_0 + 2\gamma) = 3.76\phi_0$. This result is also in good agreement with the experimental data, even at large d, since the best fit in Fig. 3 gives $\phi(0) = 3.73\phi_0$. It is worth noting that these results are valid for elastic deformations. The global shape of the d cone, however, as shown in Figs. 4 and 2, is due to geometric constraints. In Sec. V we will study the geometrical properties of such a cone.

V. LOCAL PROPERTIES OF THE DEVELOPABLE CONE

In this section we present the general features of the surface of a developable cone. From the profiles presented in the previous section, we can retrieve the local curvature of the concave part and the ridge (the region separating the concave region and the convex region) as well as the curvature of the crescent shape at the pushing tip. Also we will show that developable cones made from a thick sheet ($h \neq 0$) are not centered at the pushing tip. We will then define a function called the d-cone anisotropy, which measures how far the finite-thickness d cone is from the zero-thickness d cone.

A. Anisotropy

If one looks carefully at the profiles in Fig. 4, one notices that for small deformations the lines joining the convex region to the concave region are sharper than the ones corresponding to large deformations. Also the origin of the circular part of the profiles is not centered at the coordinates' origin but shifted to the right of Fig. 4. This shift is due to an anisotropy of the plate. This anisotropy is due to the fact that, when pushing the plate to make the deflection that corresponds to the d cone, the tip of the d cone obtained is then shifted to allow the deflection to form. In other terms, it costs more energy to produce a small point with a high curvature than a large deflection with small curvature. Hence, to minimize the energy necessary to make a sharp vertex, the singularity is ejected out of the plate by a distance that is, for low deformations, equal to the frame radius, and the plate surface looks smooth. The generatrices no longer meet at the pushing tip. In the following we will show how, by measuring the distance by which the origin of the cone has shifted, it is possible to characterize the deviation of the real cone from a theoretical cone. This shift can be quantified by measuring what we call the *d-cone anisotropy* $\mathcal{A}$, defined as the ratio $[\zeta(\pi) - \zeta(\pi/2)]/\zeta(\pi)$, where $\zeta(\theta)$ is the height of the sheet measured at the polar angle θ and π corresponds to the very right point in the profiles of Fig. 4.

B. Geometrical model

If we look at the d-cone ridges, where the crescent appears, we find that their loci are a plane. Furthermore, the cone generatrices do not meet at the pushing tip. From Fig. 4, we notice that the circular part, that is, the convex region, is not centered at the coordinates' origin. The obtained cone looks as if an axisymmetric cone has been cut by a plane defining then an aperture angle $2\theta_0$. In Fig. 5, we show the geometrical location where the plane and the cone meet. In the following we show the origin of this ''anisotropy'' and a geometrical scheme of the d cone.

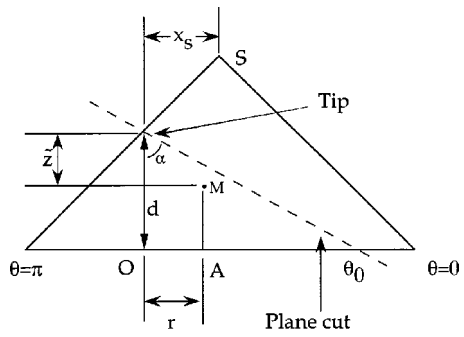

FIG. 5. Geometrical construction of the d cone obtained after a cut in the axisymmetric cone by a plane.

If S, A, and M belong to the cone, they are related by

$$\overrightarrow{SM} = \lambda \overrightarrow{SA}, \tag{5.1}$$

where S is the tip and A is on the line defined by the intersection of the moving frame and the plate of Fig. 1. If O is on the pushing line then, $\overrightarrow{OA} = R(\cos\theta \vec{i} + \sin\theta \vec{j})$. Also we have

$$\begin{aligned} \overrightarrow{SA} &= (R\cos\theta - x_s)\vec{i} + R\sin\theta \vec{j} - z_s \vec{k}, \\ \overrightarrow{SM} &= (x_m - x_s)\vec{i} + (y_m - y_s)\vec{j} + (z_m - z_s)\vec{k}. \end{aligned} \tag{5.2}$$

From Eq. (5.1) we have

$$\begin{aligned} x_m &= x_s + \lambda(R\cos\theta - x_s), \\ y_m &= \lambda R \sin\theta, \\ z_m &= (1-\lambda) z_s . \end{aligned} \tag{5.3}$$

In the previous relations, (x_m, y_m, z_m) are the coordinates of M and (x_s, y_s, z_s) are the coordinates of S. In our case R is the frame radius. One needs to find a relation between λ and θ; in fact, this can be easily achieved by calculating a distance $r^2 = x_m^2 + y_m^2$ on the cone. At r constant we have

$$\begin{aligned} &\lambda^2[(R\cos\theta - x_s)^2 + R^2\sin^2\theta] + 2\lambda x_s(R\cos\theta - x_s) \\ &\quad + x_s^2 - r^2 = 0. \end{aligned} \tag{5.4}$$

This equation gives us $\lambda(\theta)$ for a given r. The height is now given by $z_m = [1 - \lambda(\theta)] z_s$. It is more convenient to reverse the z axis and consider a direct cone so that the generatrices are in the half-plane $y > 0$ axis. We then define $z_m = d - \tilde{z}_m$ (the profiles in Fig. 4 are obtained in the reversed axis) and obtain

$$\tilde{z}_m = \lambda(\theta) d + (1 - \lambda(\theta))\tilde{z}_s . \tag{5.5}$$

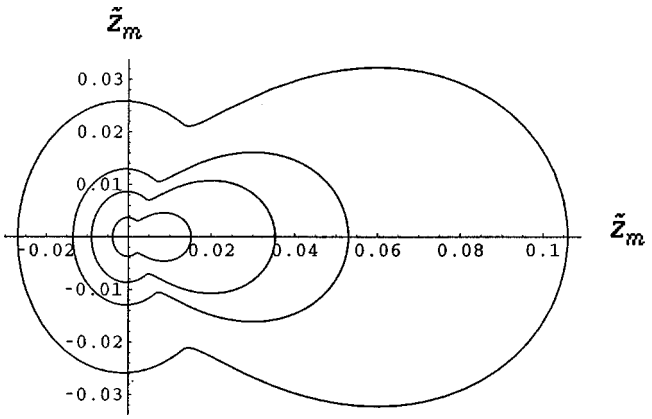

FIG. 6. Contour plot of the *d*-cone profiles obtained from Eq. (5.5). Each curve corresponds to a distance from the origin. The distance x_s is set to 1. The frame radius is set to 37 mm and the thickness to 0.1 mm. The different distances are $r=2,4,6,12$ (scaled units).

If we plot the lines $\tilde{z}(\theta)$ we recover the experimental profiles in Fig. 4. In Fig. 6, we display the profiles calculated from this model. The different profiles correspond to different distances r from the origin. The deformation is measured by calculating x_s. The frame radius is the one used in the experiments and the thickness is set to 0.1 mm. From this figure we notice that the qualitative shape of the *d* cone can be obtained from a simple geometrical model with the ansatz (4.1). In Fig. 7 we plot the height $\tilde{z}_m$ versus the polar angle θ. From this figure the opening angle is equal to 114°. The aperture angle is selected geometrically.

The cut in Fig. 5 then defines a hyperbola whose equation is obtained from the following construction: The plane when cutting the cone defines an angle α, so that $\tan\alpha = x_m/(z_m - d) = -(R\cos\theta_0)/d$. The intersection of the plane and the cone is given by.

$$X = \lambda R \sin\theta,$$

$$Y = -(1/\sin\alpha)[x_s(1-\lambda) + \lambda R\cos\theta], \tag{5.6}$$

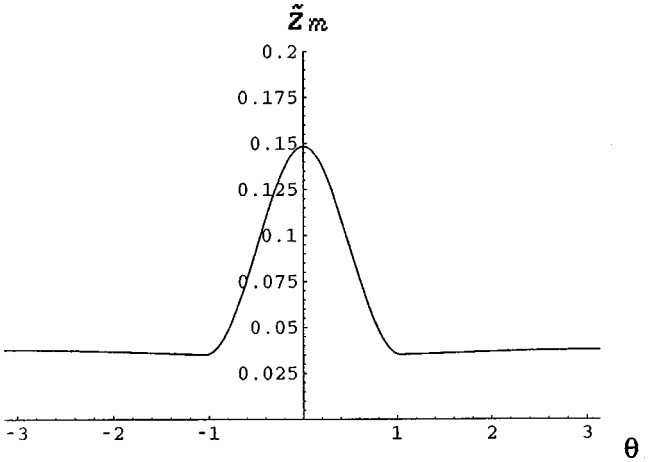

FIG. 7. The plate height $\tilde{z}_m$ obtained from the geometrical model. The parameters are the same as in Fig. 6. The distance to the tip is two scaled units.

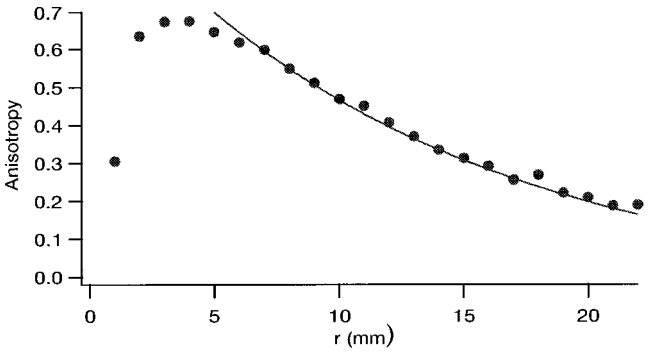

FIG. 8. The anisotropy $\mathcal{A}$ as a function of the distance r. The deformation is 1.5 mm.

with

$$\lambda(t) = [(z_s - d)\tan\alpha - x_s]/(R\cos t - x_s + z_s\tan\alpha). \tag{5.7}$$

Eliminating $\lambda(t)$ between Eqs. (5.6) and (5.7) we find

$$X^2\left(1+\frac{x_s}{R}\right)^2(d^2+R^2\cos^2\theta_0) + Y^2[(x_s+(R+x_s)\cos\theta_0]^2 - R^2 - 2YX_s(R+x_s)(1+\cos\theta_0) - \sqrt{d^2+R^2\cos^2\theta_0} = 0. \tag{5.8}$$

Equation (5.8) is the equation of a hyperbola whose curvature at the tip is given by

$$\kappa = \frac{(R+x_s)\sqrt{d^2+R^2\cos^2\theta_0}}{R^2x_s(1+\cos\theta_0)} \sim \frac{1}{2x_s} \quad (x_s \ll R). \tag{5.9}$$

We showed that with this one-dimensional geometrical model we can characterize the size of the singularity, and found that it belongs to a hyperbola defined as the intersection of a plane with a perfect cone. For a ''real'' sheet, it is energetically favorable to create a deflection by bending and rejecting the singular point far away from the tip and to have the obtained *d* cone not have a singular tip or a vertex.

C. The shift from the anisotropy

From Fig. 5 the angle α is given by $\tan\alpha = d/R$, so that $z_s = -x_s\tan\alpha$. We define the anisotropy $\mathcal{A}(r, R_f, x_s)$, keeping in mind that the deflection is centered at $\theta = 0$:

$$A = [\tilde{z}(\pi) - \tilde{z}(\pi/2)]/\tilde{z}(\pi) = [-rR + x_s(r-R) + \sqrt{B}]/r(x_s - R), \tag{5.10}$$

where $B = r^2R^2 - x_s^2(r^2 - R^2)$. The distance x_s is obtained by measuring the heights from the profiles, such as the ones depicted in Fig. 4, and fitting the data with expression (5.10), giving the anisotropy versus the frame radius R_f and the distance r. In Fig. 8, we show an example of the anisotropy measured from the profiles, where the line is the best fit with the formula (5.10) for a given deformation. The anisotropy, found experimentally, decreases when increasing r. This effect is due to the fact that, close to the singularity, the plate suffers a stress focusing, and an irreversible deformation, due

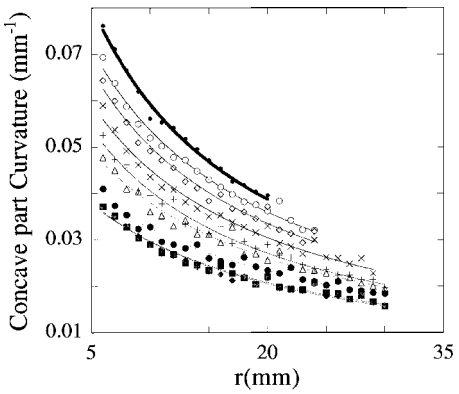

FIG. 9. Concave-part local curvature versus the distance to the singularity, for different small d. The line is a best fit to the function $1/(r+r_s)$.

to stretching, would take place if we increased the deformation. Further away from the singularity, the plate surface suffers pure bending.

In the next section we will show that the local curvature of the concave part does not follow a law of the form $1/r$, but the coordinates are shifted by a value we call r_s that depends on the deformation. The shift in coordinates' origin r_s is correlated to the displacement of the singularity x_s. We will show, that due to stress focusing, this distances decrease when the deformation is increased.

D. Size of the singularity and stress focusing

We have measured the local curvature of the concave region and found that, for small deformations, the radius of curvature is linear with the distance from the tip, but the origin is shifted by r_s. It is well known that at each point of a perfect cone there is no curvature towards the vertex. The curvature decreases like $1/r$, where r is the distance from the vertex. In Fig. 9, we display the local curvature versus the distance from the pushing tip. The line is the best fit to a function of the form $1/(r+r_s)$. From Fig. 9 the origin of the coordinates is not centered at the pushig tip, but is shifted by a distance r_s. This distance is found to be a decreasing function of the deformation as well as the distance x_s. This shift in the cone origin is due to the fact that it is cheaper to make a bent smooth surface than a sharp pointlike vertex with a high curvature. As a result of the stress focusing, the size of the singularity, which at small deformations has a size of the same order of magnitude as the frame radius, decreases when the deformation increases. In Fig. 10 we depict x_s and r_s versus the deformation.

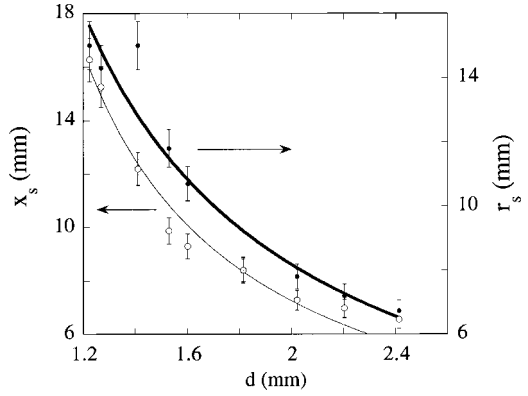

FIG. 10. The shift distance r_s and the singularity displacement x_s versus d.

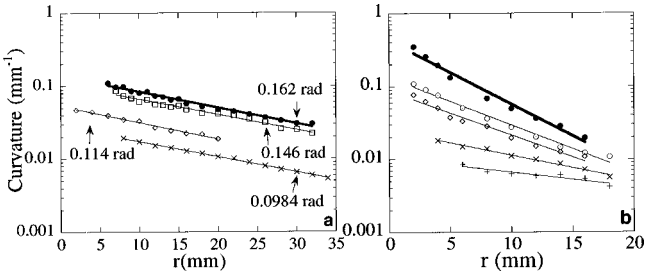

FIG. 11. d-cone local curvature versus the distance r from the pushing tip for different deformations. (a) The local curvature of the concave part, where r_c is constant and equal to 20 mm. (b) The ridge local curvature, where r_c decreases when d increases. We reported the values of the opening angle and not d.

Notice that both r_s and x_s decrease when the deformation is increased. As the bending rigidity acts like h^3 where h is small, the creation of a punctual singularity costs more energy than making a simple deflection by bending the surface. From Fig. 10 we notice that at small deformations the singularity is rejected to infinity. The size of the singularity is of the order of magnitude of R_f or even larger. When the deformation increases, the size of the singularity decreases by increasing the distances x_s and r_s. The stress focusing can be seen as a decrease in the singularity size by strain localization.

E. Curvature at high deformation: Stretching effect

As we increase the deformation, a line with a different texture from the rest of the plates appears at the ridges, and the curvature increases. In order to characterize this transition we measured the curvature at high deformations, both in the concave region and at the ridge. In Fig. 11 we show the curvature of the concave region (a) and of the ridge line (b). Each data set corresponds to a given deformation.

From Fig. 11 we notice that the curvature is no longer of the form $1/r$ but decreases exponentially with the distance, like $C_0 e^{(-r/r_c)}$, where r_c is a characteristic distance. In Fig. 11(a) the characteristic distance r_c is constant versus the deformation, whereas on the ridge of Fig. 11 r_c decreases with increasing the deformation. This behavior is due to the fact that the crescent appears only on the ridge. In other words, the plastic deformation induced by stretching is felt on the ridge where the plate is folded and where the stress is concentrated. The slope of the top line in Fig. 11(a) reaches a value that corresponds to the radius at which the yield limit of a 0.1-mm-thick copper sheet is exceeded and where a permanent scar appears [18].

The deviation of the curvature from $1/r$ behavior to an exponential is due to the fact that at large d the yield limit of the material is exceeded and stretching starts to be more important than pure bending because, contrary to a free sheet, the latter system is squeezed within a circular frame. This fact explains why the stretching effects are noticeable and the deflection near the borders looks rather more flattened than if the d cone were border-free. As a first approxi-

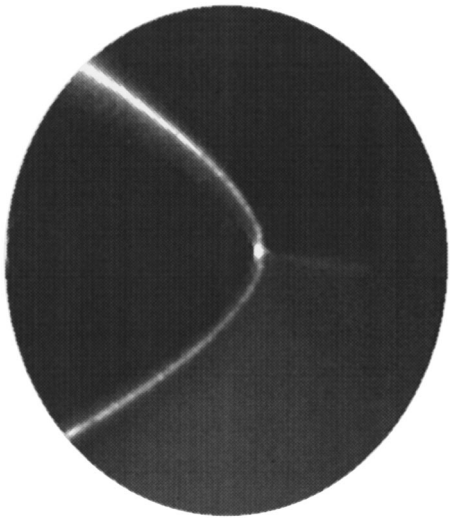

FIG. 12. *d* cone observed from above, and illuminated perpendicularly to the plane of the bright parabola. The deformation is about 0.3 mm. $R_f = 22.5$ mm.

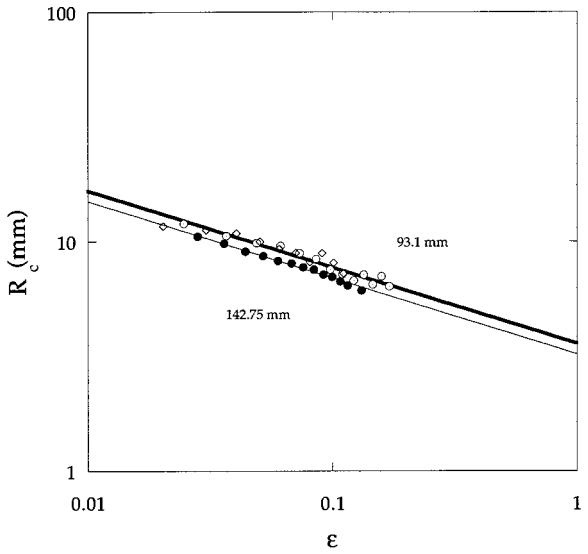

FIG. 13. Radius of curvature of the crescent for small ϵ. The line is a best fit to the power law $\epsilon^{-1/3}$.

mation we assume that concave part is an isolated stripe. By further pushing the plate beyond the yield limit the stripe starts to bend and the region near the singularity at the pushing tip suffers stretching. Following [19], if we include stretching in the energy balance we find that the stripe local curvature decreases like an exponential, and the cutoff distance decreases by increasing the height of the sheet [12]. The curve giving the curvature versus the distance for a *d* cone made of a 0.05-mm-thick sheet gives a cutoff distance that is half of the distance for a 0.1-mm-thick sheet. We noticed no qualitative changes between the two plates, and we believe that the cutoff distance is a linear function versus the plate thickness *h*. Another way to characterize the singularity size is to measure the properties of the crescent shape observed at the pushing tip.

F. The crescent singularity

Crumpling a thin sheet or a transparency leaves scars that looks like crescents. These crescents are the result of stress focusing. One wonders why the scars where the stress is focused stress are not pointlike. This is due, as discussed above, to the fact that making a singularity whose radius of curvature is of the order of *h* costs more energy than pure bending. It is to be kept in mind that the only natural length scale is the thickness. Instead, it is preferable to make a crescent whose spatial extension is orders of magnitude larger than *h*. It is then of great importance to measure the size of the crescent left after crumpling. In our experiment, we measured the radius of curvature R_c of the crescent as a function of the deformation for small and large deformations.

1. Radius of the parabola for low deformations

To measure the crescent radius of curvature, we illuminate the *d* cone from above, so that the light beam is perpendicular to the ridge. The ridge reflects more light than the rest of the plate, as its texture is affected by the bending. Figure 12 displays the *d* cone for a small deformation. Notice the parabolic shape of the bright line separating the convex region from the concave region. This line defines an angle smaller than $2\theta_0$ defined in Sec. III. The image looks oval, because as the plane defined by the parabola makes an angle $\pi/2-\alpha=\arctan\epsilon$ with the horizontal plane, the frame is twisted by the same angle so that the light beam is perpendicular to the parabola (α is defined in Fig. 5 where the opening angle is exaggerated).

We digitalize the image and collect the points belonging to the bright line. We have then a parabola whose radius of curvature can be easily estimated by fitting the obtained curve to a second-order polynomial [14,15].

Figure 13 depicts the radius of curvature of the bright parabola in Fig. 12 as a function of $\epsilon=d/R_f$. We show the data in a linear scale for the sake of clarity. We observe that the radius of cuvature of the crescent scales like $\epsilon^{-1/3}$, where ϵ is defined above. In this regime, the deflection is moving downward. This motion is due to the reaction force experienced by the plate at the point where the plate loses contact with the frame.

2. The radius of the crescent at high deformations

We have measured the curvature of the crescent at high deformations too. In this case the ridge is a thin line and its shape is no longer a parabola. It has a shape of a hyperbola, whose wings are likely to be linear. To find the crescent radius of curvature, we follow the same method for fitting as above. A *d* cone at large deformations and highlighted from above is displayed in Fig. 14, where we notice that the bright line separating the convex region and the concave region looks like a hyperbola and defines a sharp ridge near the pushing tip (this region is the core region or the singularity region). Beyond a certain distance from the core region, the line becomes straight [20]. The radius of the crescent is measured by fitting the line in the core region to a polynomial. In Fig. 15, we show the radius of curvature of the crescent for $\epsilon>0.1$. The fitting procedure does not depend on the polynomial degree we use to make the fitting. The lines in Fig. 15 are power laws with an exponent $-1/2$. In the following we present a model based on a competition between pure bending and pure stretching but in the region that bounds the crescent.

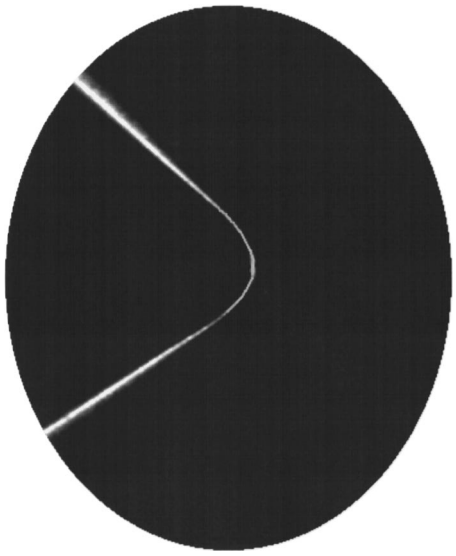

FIG. 14. Top view of the d cone at high deformation. For the bright line, which is no longer a parabola, but a hyperbola, one can notice a distance over which the wings of this line become linear. The deformation is about 7 mm. $R_f=30$ mm.

3. Scaling for high deformations

In this section we will show that the power law can be found by considering that the concave region near the pushing tip, besides being stretched, is bent as well. We also consider that the invagination is no longer moving downward, but the ridges are approaching each other too. To do so let us write the bending energy

$$E_{\text{ben}}=\kappa\int(\nabla^2\xi)^2dS \tag{5.11}$$

and the stretching energy for such a plate:

$$E_{\text{str}}=G\int(\nabla^2\chi)^2dS. \tag{5.12}$$

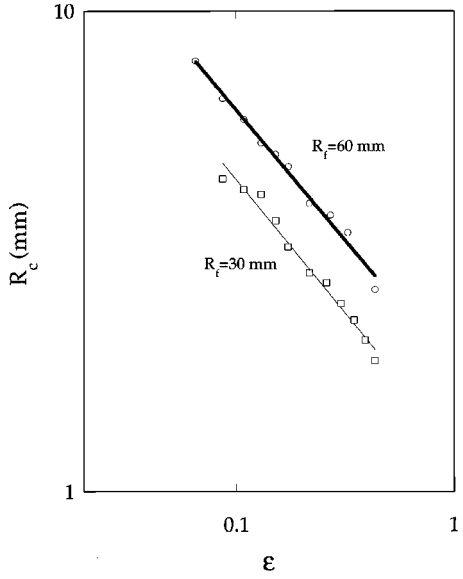

FIG. 15. Radius of the crescent versus ϵ for large deformations. The lines are best fit to the power law $\epsilon^{-1/2}$.

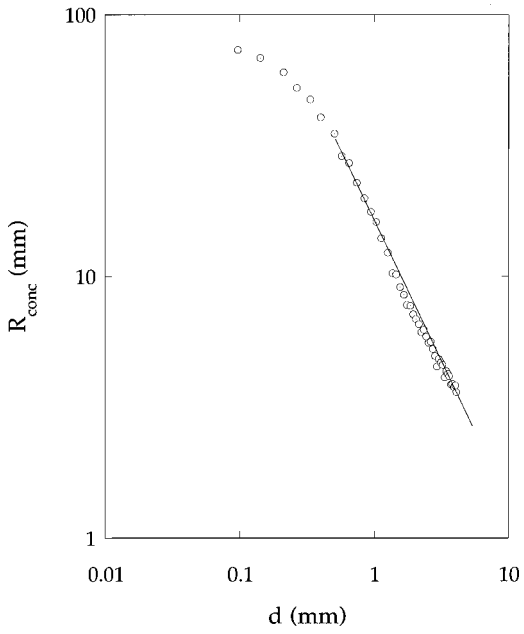

FIG. 16. Local radius of curvature of the concave region close to the singularity. The line has a slope close to -1.

Here χ is the Airy function, κ is the bending rigidity, and G is the stretching modulus related to κ for two-dimensional plates by $G\simeq\kappa/h^2$ where h is the thickness. If we suppose that all the stretching in the line that delimits the concave part and the convex part (ridge) is due to bending at the tip, the curvature $\nabla^2\xi$ can then be written as d/R_c^2. We integrate the bending energy over the surface R_fR_c. Hence, the bending energy is

$$E_{\text{bend}}\sim\kappa(d/R_c^2)^2R_fR_c\sim\kappa d^2R_fR_c^{-3}. \tag{5.13}$$

For the stretching energy we keep the same surface of integration. The strain created by the decay of the curvature is due to the fact that the sheet is loaded by a small angle ϵ. The plate experiences a force F when creating the deflection along the radius R_f; the plate then has a moment at the tip FR_f. For high deformations, not only does the deflection move downward but the two ''wings'' start to approach each other in the azimuthal direction, which creates a characteristic strain $\gamma=(d^2/R_f^2)^2$. The stretching energy is then

$$E_{\text{str}}\sim\kappa/h^2(d^2/R_f^2)^2R_fR_c\sim\kappa h^{-2}d^4R_f^{-3}R_c. \tag{5.14}$$

Minimizing $E_{\text{bend}}+E_{\text{str}}$ with respect to R_c, we find that.

$$R_c\sim R_f\sqrt{h/d}. \tag{5.15}$$

Knowing that $\epsilon=d/R_f$,

$$R_c\sim\sqrt{R_fh/\epsilon}. \tag{5.16}$$

If we consider the tip of the d cone as the core of a dislocation whose bending energy is logarithmic [9,16], and if one considers two types of stretching (radial and azimuthal), one recovers the scaling of a d cone obtained by squeezing a sheet in a cone of revolution, i.e, $R_c\sim1/\epsilon$. This scaling is probably due to the fact that the only scaling in this particular problem, apart from the thickness, is the opening

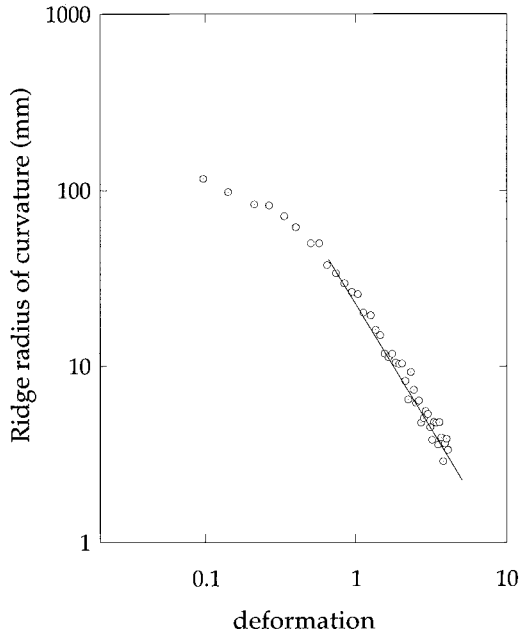

FIG. 17. Radius of curvature of the ridge as a function of the deformation. The straight line has a slope -1.5.

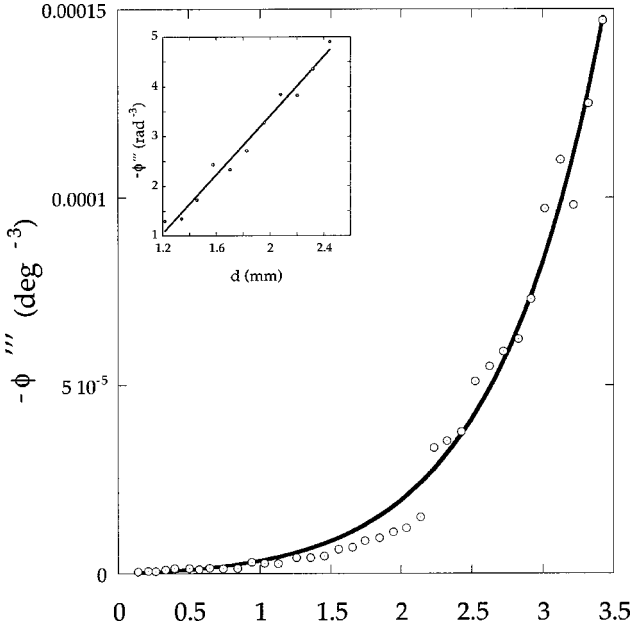

FIG. 18. Third derivative of the profile (ϕ) at the ridge versus the deformation and at a distance of 3 mm from the tip. Inset: the third derivative at a distance of 6 mm from the *d*-cone tip.

angle of the squeezing cone. In Fig. 16 we show the radius of curvature of the *d* cone concave part close to the pushing tip. For large deformations the radius scales like ϵ^{-1}.

One possible way to observe stress focusing is by comparing the growth of the curvature between the concave region and the ridge. In Fig. 17 we plot the radius of curvature at the ridge versus the deformation, and the slope of the line is equal to -1.5. The fact that the radius of curvature at the ridge decreases faster than the radius at the concave region is also an indirect measurement of stress focusing inducing a curvature focusing. In the next section we will show how from the profiles one can also observe stress focusing by measuring the reaction force at the ridge and at the concave part.

VI. SINGULARITY ENERGY AND FORCE MEASUREMENTS

The crumpled paper is similar to the discovery of Laplace and best known as the ''plateau problem,'' which consists in the determination of minimal surface, given its border (soap film); whereas in the crumpling problem, the volume is kept fixed; that is, when making a ball by crumpling a piece of paper, the stress is distributed over the regions where the sheet is ''postbuckled.'' The *d*-cone problem is much simpler than the real crumpled paper. As discussed above, it consists of fixing a border, i.e., the frame radius (Fig. 1) and squeezing a sheet into it. The force applied to the center of the plate is responsible for the creation of the torque that causes the plate to deflect and gives rise to the ''*d* cone.'' In this section we discuss the results of the response of the plate to the external load at its center.

A. Torque from profiles

In this section we will determine the reaction forces experienced by the plate at the borders as a result of the external load (F). The resultant of these forces is equal to the external loading; we will determine the force at the ridge where most of the stress is concentrated (Fig. 2). It is well known in classical mechanics that the force acting in a certain direction is equal to the derivative of the energy with respect to the coordinate in this direction. In our case, the reaction force experienced by the plate at the border where it is deflected is defined by the derivative of the energy with respect to the displacement ζ. The plate resists bending by a reaction force:

$$F_{\text{reac}}=\frac{\partial E_b}{\partial \zeta}\sim \frac{1}{\zeta'}\frac{\partial}{\partial \theta}\int \left(\frac{\partial^2 \zeta}{\partial \theta^2}\right)^2 d\theta. \tag{6.1}$$

Integrating by part we find

$$F_{\text{reac}}\sim -\frac{1}{\zeta'}\frac{d}{d\theta}\int \zeta'\zeta''' d\theta \tag{6.2}$$

$$\sim -\zeta'''=-r\phi'''=-r\frac{\partial^3 \phi}{\partial \theta^3}. \tag{6.3}$$

In Fig. 18 we display the third derivative of the profile at the ridge. To measure the reaction force we derive the profile twice versus the angle θ and we calculate the slope of the straight line where the curvature $\sim\zeta''$ varies. The force is supposed to increase linearly for small deformations when the regime is still elastic. From Fig. 18, ϕ''' enlarges exponentially; we believe that this is due to the plastic transition. However, far away from the singularity the force increases linearly, even for large deformations. The fit in Fig. 18 is of the form $(de^{d/a}-1)$, whereas the fit in the inset is a linear fit.

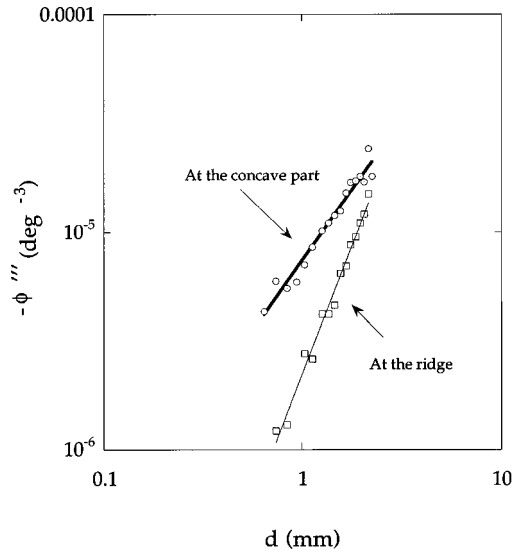

FIG. 19. Reaction force at the ridge and at the concave part vs the deformation. The slope of the line giving the force at the ridge is twice as larger as the one corresponding to the concave part. The data are taken at 3 mm from the tip.

The exponential behavior of the force is also a measure of the force focusing that creates the crescent near the tip. The exponential behavior was observed in the behavior of the curvature for high deformations [Fig. 11] and was explained as a consequence of geometry-induced stretching. To satisfy energy considerations and to verify scaling considerations, this curvature was found to decay exponentially [12]. The reaction force ($\sim|\phi'''|$) far from the singularity is linear over the same range of deformation (inset of Fig. 18). Two regions experience reaction forces and then torque, which gives rise to the invagination. These two regions are the ridge, and the concave part. It can be easily observed that the ridge experiences more stress than the concave part. In Fig. 19 we display $|\phi'''|$ at the ridge and at the concave region. The slope of the fitting line in the case of the reaction force at the ridge is larger than the one corresponding to the concave part. It is clear then that the stress due to the reaction force increases faster at the ridge than at the concave part. The stress is focused at the ridges where the crescent nucleation takes place. Since the plate is more deflected far away from the singularity than closer to it, we have measured the reaction force as a function of the distance from the singularity for two different deformations. We would have a linear behavior for the reaction force if only bending were present, but as the plate may be stretched, we have a nonlinear increase of the reaction force. However, the behavior of the reaction force seems to be the same for the two distances. In the following subsection, we discuss a measure of the force experienced by the plate at its tip.

B. Direct force measurements

As long as long the deformation is kept small during the loading, a deflection appears and neither a singularity nor a sharp ridge is observed; this regime is elastic, and bending dominates over stretching. The force exerted by the plate is linear in the deformation. As we increase the load, the line at the ridge becomes sharper and the force is no longer linear; the regime is plastic and stretching becomes comparable to bending. In Fig. 20, we display the force versus ϵ. It is clear that the opening angle defined by ϵ at which the force saturates is the same for the different frame radii. However, the maximum force at saturation is large for smaller frames. Also, it is worth noting that the force changes its slope around $\epsilon \simeq 0.1$ for transparencies; this corresponds to the same value where we have observed a crossover between the $-1/3$ and the $-1/2$ scaling of the crescent radius versus ϵ.

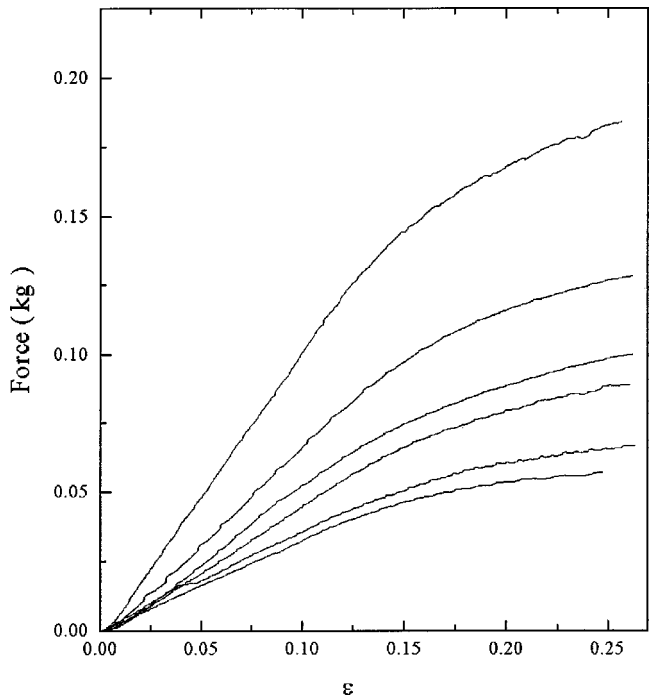

FIG. 20. Force vs ϵ for different frame radii for transparencies. The saturation force increases when the frame radius decreases.

In Fig. 20 the maximum force at which the plate saturates scales with the frame radius like $F_{\mathrm{sat}} \sim R_f^{-0.77}$. For low deformations the force is linear with the deformation where only bending is dominant. If we assume that in the elastic regime, the work necessary to load the plate by a distance d is (Fd) and is equal to the bending energy that is proportional to d^2/R_f^2 (to be integrated over the plate surface R_f^2), we find that $F \sim d/R_f^2$. This result is in agreement with the behavior of the reaction force in Fig. 18. In Fig. 21 we plot the slope F/d of the linear part of the force versus the frame radius. The slope of the fitting line is close to 2. From this scaling, the force goes like ϵ/R_f. Now we are able to measure the energy necessary to create the crescent line. In the following we show how we measure this *singularity energy*.

C. Singularity's energy

When a thin plate is bent elastically and released, it recovers its original shape. But, if the plate is bent until the internal face experiences compression and the external face experiences stretching, the plate will have deformed plastically and will not recover its shape. In force measurements, the load necessary to bend the plate to the same point, in subsequent tests will be lower because the plate has been ''weakened.'' In order to measure the singularity energy, we first measure the force required to reach a deformation z^*,

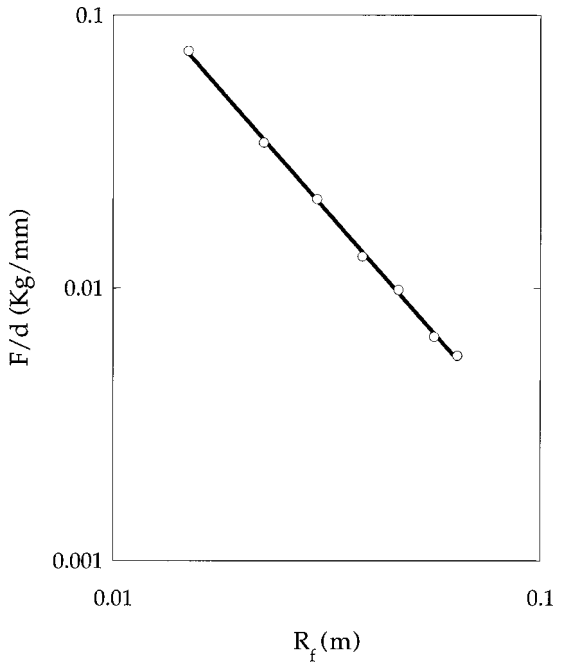

FIG. 21. Slope of the force in the elastic regime vs R_f. The slope of the fitting line is close to 2.

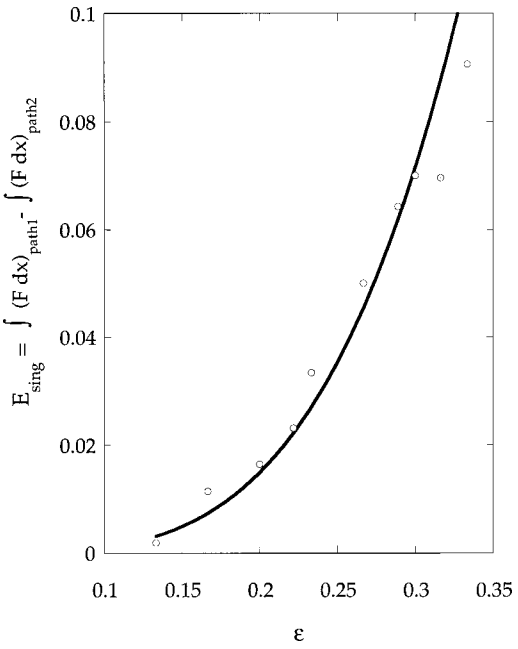

FIG. 23. Singularity energy, which is the energy necessary to form the scar versus the deformation. The line is the best fit to a power law ϵ^4.

then release the plate, and measure the force required to reload the plate to the deformation z^*. The area between the loading lines, shown in Fig. 22, is the singularity energy, corresponding to the energy dissipated while creating the scar region. If the plate is loaded a third time, the force follows the loading line corresponding to the second loading.

If z is the displacement variable, then the singularity energy is given by

$$E_{\text{sing}} \simeq \int_0^{z^*} (F_1\, dz)_{\text{Path 1}} - \int_0^{z^*} (F_2\, dz)_{\text{Path 2}}, \qquad (6.4)$$

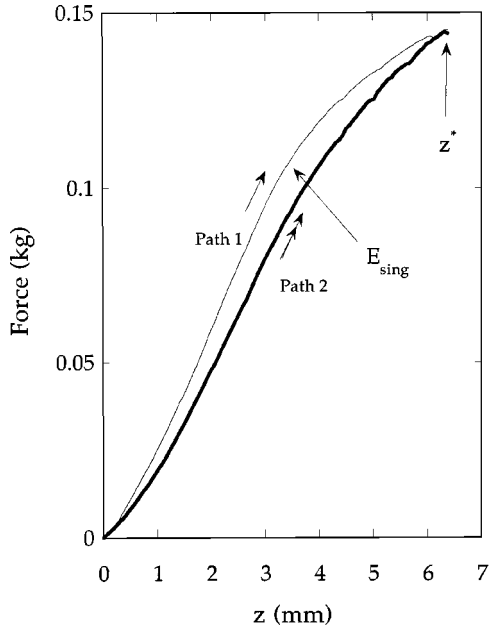

FIG. 22. Method by which the energy of the singularity is measured. Path 1 and Path 2 are the buckling of a perfectly flat plate and the reloading of the already buckled plate. The area between the thick line (Path 2) and the thin line (Path 1) is the energy of the singularity.

where Path 1 and Path 2, correspond to the first and second loadings. F_1 and F_2 are the force on an undeformed plate and the force on an already deformed plate, respectively. For subsequent loadings after the initial loading, the force always follows Path 2 as long as the deformation does not exceed z^*. To measure the friction of the border on the plate, we ''unload'' the plate, and for the same deformation, the force shows a sharp drop. This drop in the force is due to friction and is not taken into account, as it is eliminated when calculating the surface separating the two loads. Figure 23 shows the singularity energy as a function of $\epsilon = z^*/R_f$. The line is a power law ϵ^4.

Ben Amar and Pomeau [9], showed that the stress in the inner region where the nonlinear effects are dominant is proportional to ϵ^2. In their case, the total energy was reduced to the stretching energy: $\int (\partial^2 \chi/\partial x_i \partial x_j)^2 dS \simeq \int \sigma_{ij}^2 dS$. They have neglected the bending energy, as it is proportional to h^3, and because any other length scale in the problem is much bigger than h. For large deformations, this assumption is valid, because the frame radius is the most important length scale in the problem as it works to squeeze the plate. The energy needed to deform the plate can also be considered to be the ''developable cone energy,'' since the plate cannot recover its original shape after forming a developable cone. If one isolates the scar region, however, by cutting a circular region around the singularity, the outer band becomes flat. Since the scar region forces the plate to assume the conical form, we conclude that all of the dissipated energy is concentrated in the scar region and thus this ''developable cone energy'' is also equated with the ''singularity energy.''

VII. DISCUSSION

In this paper we explored properties of the conical singularity in a buckled thin elastic sheet. This singularity is known as the developable cone that may be relevant to a description of crumpled elastic membranes. Profiles of the surface were studied. The relation between the maximum deflection and the deformation imposed on the plate was derived. We have measured the geometrical or spatial deviation of the conical singularity made of real sheets ($h \neq 0$) from a theoretical one. We called this deviation the anisotropy of the plate. This anisotropy is a geometrical anomaly related to the rejection of the region far from the plate that minimizes energy and where the stress is focused. The aperture angle of the *d* cone was measured and found to be universal and depends only on the geometry of the frame. A simple model based on the minimization of the curvature energy for an isometric deformation was sufficient to describe the region outside the singularity. Also the shape of the *d* cone obtained from profilometry measurements was reproduced using a simple geometrical model. The curvature at the ridge and at the concave part were both measured, and a stress focusing was observed of a fast decrease of the radius of curvature at the ridge in comparison to the curvature of the concave region. From the profiles, it was possible to quantify the reaction force and describe how the stress is focused at the ridge where the scar appears in the form of a crescent. This crescent has a curvature that scales with the deformation experienced by the plate. Two regimes were found. At small deformations the crescent has a parabolic form whose radius varies slowly with the deformation and whose singularity size is of the order of the frame radius. At higher deformations, the crescent is squeezed and is no longer a parabola, and its radius varies faster with the deformation; the singularity is confined to a smaller region around the tip. From load measurements, the scaling of the force in the elastic regime versus the deformation and the frame radius was found. The two different scalings of the crescent radius versus the deformation arise from the fact that at small deformations and when the force is linear in the deformation the plate is bent and no sharp ridge is observed while the aperture angle $2\theta_0$ remains constant. Beyond the crossover where $\epsilon \simeq 0.1$ and where the force changes its slope, the mechanism is no longer the same: the two ridges approach each other, the crescent is itself folded in the azimuthal direction, and the aperture angle decreases. The scaling of the crescent curvature versus the deformation is not universal. It was also possible to measure the energy needed to create the scar. We called this energy the *singularity energy*. This energy was measured as the energy dissipated in the plate to form the scar. The stress focusing inducing a curvature focusing and an increase in the singularity energy is similar to the defect-induced dislocation in the liquid crystal, where the spatial extension of the defect when squeezed into a smaller region is decreased and the curvature of the molecular planes increases. In fact, if we look at a smectic layer in the vicinity of a core of parabolic domain, we can notice that this layer defines an object similar to a *d* cone. In this experiment the stress focusing induces a strain localization near the singularity.

Apart from the analogy between the logarithmic divergence of the curvature energy, the deflection resembles Orowin's analogy of the motion of a snake or a carpet [16]. The strength of the dislocation in this case is measured by the maximum deflection.

Although crumpled vesicles have been observed [1], no systematic local study of the surface of a crumpled vesicle has been performed. Profilometry using a laser beam or magnetic beads on the surface of a crumpled vesicle can complement freeze fracture microscopy experiments usually used to probe vesicles in suspensions. It is known that the crease's nucleation in a buckled plate is subcritical and the formation of the singularity that bounds a crease is sudden; it is then of great importance to study topological properties of such singularities at subcriticality [14]. In the experiment described above, the appearance of the invagination for small-diameter sheets is sudden and subcritical. It is of interest to study the emission of sound when the sheet buckles. Also, in real crumpled sheets, singularities may interact, giving rise to a rich behavior, such as the one encountered in the physics of defects. This latter point is the subject of a future publication.

ACKNOWLEDGMENTS

We thank Jean-Christophe Géminard for his valuable collaboration in Secs. IV and V A–V C. This work was financed in part by the DICyT of the University of Santiago, Under Grant No. 049631CH, and by a ''Catedra Presidencial en Ciencias.''

[1] M. Mutz, D. Bensimon, and M.J. Brienne. Phys. Rev. Lett. **67**, 923 (1991).

[2] Y. Kantor, M. Kardar, and D.R. Nelson, Phys. Rev. Lett. **57**, 791 (1986); *Statistical Mechanics of Membranes and Surfaces*, edited by D. Nelson, T. Piran, and S. Weinberg (World Scientific, Singapore, 1989).

[3] D.R. Nelson and L. Peliti, J. Phys. (Paris) **48**, 1085 (1987); M. Paczuski, M. Kardar, and D.R. Nelson, Phys. Rev. Lett. **60**, 2638 (1988); D. Morse, T. Lubensky, and G. Grest, Phys. Rev. A **45**, R2151 (1992); D. Bensimon, D. Mukamel, and L. Peliti, Europhys. Lett. **18**, 269 (1992); X. Wen, C.W. Garland, T. Hwa, M. Kardar, E. Kokufuta, Y. Li, M. Orkisz, and T. Tanaka, Nature (London) **355**, 426 (1992); R. Attal, S. Chaïeb, and D. Bensimon. Phys. Rev. E **48**, 2232 (1993); Y. Park and C. Kwon, *ibid.* **54**, 3032 (1996).

[4] M.S. Spector, E. Naranjo, S. Chiruvolu, and J.A. Zasadzinski, Phys. Rev. Lett. **73**, 2867 (1994); R.R. Chianelli, E.B. Prestige, T.A. Pecoraro, and J.P. DeNeufville, Science **203**, 1105 (1979).

[5] M.R. Falvo, G.J. Clary, R.M. Taylor II, V. Chi, F.P. Brooks, Jr., S. Washburn, and R. Superfine, Nature (London) **389**, 582 (1997); M.M.J. Treacy, T.W. Ebbesen, and J.M. Gibson, *ibid.* **381**, 678 (1996); B.I. Yakobson, C.J. Brabec, and J. Bernholc, Phys. Rev. Lett. **76**, 2511 (1996).

[6] S. Deser, R. Jackiw, and G. 't Hooft, Ann. Phys. (N.Y.) **152**, 220 (1984).

[7] A. Lobkovsky, S. Gentges, H. Li, D. Morse, and T.A. Witten, Science **270**, 1482 (1995).
[8] Y. Pomeau, C. R. Acad. Sci., Ser. I: Math. **320**, 975 (1995).
[9] M. Ben Amar and Y. Pomeau, Proc. R. Soc. London, Ser. A **453**, 729 (1996).
[10] T.A. Witten and H. Li, Europhys. Lett. **23**, 51 (1993).
[11] E.M. Kramer and T.A. Witten, Phys. Rev. Lett. **78**, 1303 (1997).
[12] A. Lobkovsky, Phys. Rev. E **53**, 3750 (1996);
[13] A.E. Lobkovsky and T.A. Witten Phys. Rev. E **55**, 1577 (1997).
[14] S. Chaïeb and F. Melo, Phys. Rev. E **56**, 4736 (1997).
[15] S. Chaïeb, F. Melo, and J.C. Géminard, Phys. Rev. Lett. **80**, 2354 (1998).
[16] E. Cerda and L. Mahadevan, Phys. Rev. Lett. **80**, 2358 (1998).
[17] S. Chaieb, F. Melo, and J-C. Géminard (unpublished).
[18] S. Chaieb and F. Melo, *in Instabilities and Nonequilibrium Structures VI*, edited by E. Tirapegui and W. Zeller (Kluwer, Dordrecht, 1997).
[19] L. Landau and E. Lifchitz, *Théorie de l'Élasticité* (Mir, Moscow,1967), p. 87.
[20] The term (wing) is introduced in [13] to describe the region where the strain persists, although all the energy is concentrated near the singularity.